

Somatic Oxidative Bioenergetics Transitions into Pluripotency-Dependent Glycolysis to Facilitate Nuclear Reprogramming

Clifford D.L. Folmes,¹ Timothy J. Nelson,^{1,2} Almudena Martinez-Fernandez,¹ D. Kent Arrell,¹ Jelena Zlatkovic Lindor,¹ Petras P. Dzeja,¹ Yasuhiro Ikeda,³ Carmen Perez-Terzic,^{1,4} and Andre Terzic^{1,5,6,*}

¹Center for Regenerative Medicine and Marriott Heart Disease Research Program, Division of Cardiovascular Diseases, Department of Medicine

²Transplant Center and Division of General Internal Medicine, Department of Medicine

³Department of Molecular Medicine

⁴Department of Physical Medicine and Rehabilitation

⁵Department of Molecular Pharmacology and Experimental Therapeutics

⁶Department of Medical Genetics

Mayo Clinic, Rochester, MN 55905, USA

*Correspondence: terzic.andre@mayo.edu

DOI 10.1016/j.cmet.2011.06.011

SUMMARY

The bioenergetics of somatic dedifferentiation into induced pluripotent stem cells remains largely unknown. Here, stemness factor-mediated nuclear reprogramming reverted mitochondrial networks into cristae-poor structures. Metabolomic footprinting and fingerprinting distinguished derived pluripotent progeny from parental fibroblasts according to elevated glucose utilization and production of glycolytic end products. Temporal sampling demonstrated glycolytic gene potentiation prior to induction of pluripotent markers. Functional metamorphosis of somatic oxidative phosphorylation into acquired pluripotent glycolytic metabolism conformed to an embryonic-like archetype. Stimulation of glycolysis promoted, while blockade of glycolytic enzyme activity blunted, reprogramming efficiency. Metaboproteomics resolved upregulated glycolytic enzymes and downregulated electron transport chain complex I subunits underlying cell fate determination. Thus, the energetic infrastructure of somatic cells transitions into a required glycolytic metabolite to fuel induction of pluripotency.

INTRODUCTION

Stemness transcription factors reprogram somatic cell fate to achieve embryonic-like pluripotency, the hallmark of induced pluripotent stem cells (iPSC) (Takahashi and Yamanaka, 2006; Meissner et al., 2007; Nelson et al., 2010). Developmental metabolic plasticity is associated with pluripotent stem cell fate specification (Dzeja et al., 2011), yet the metabolic dynamics that match the bioenergetic demand of nuclear reprogramming have not been established.

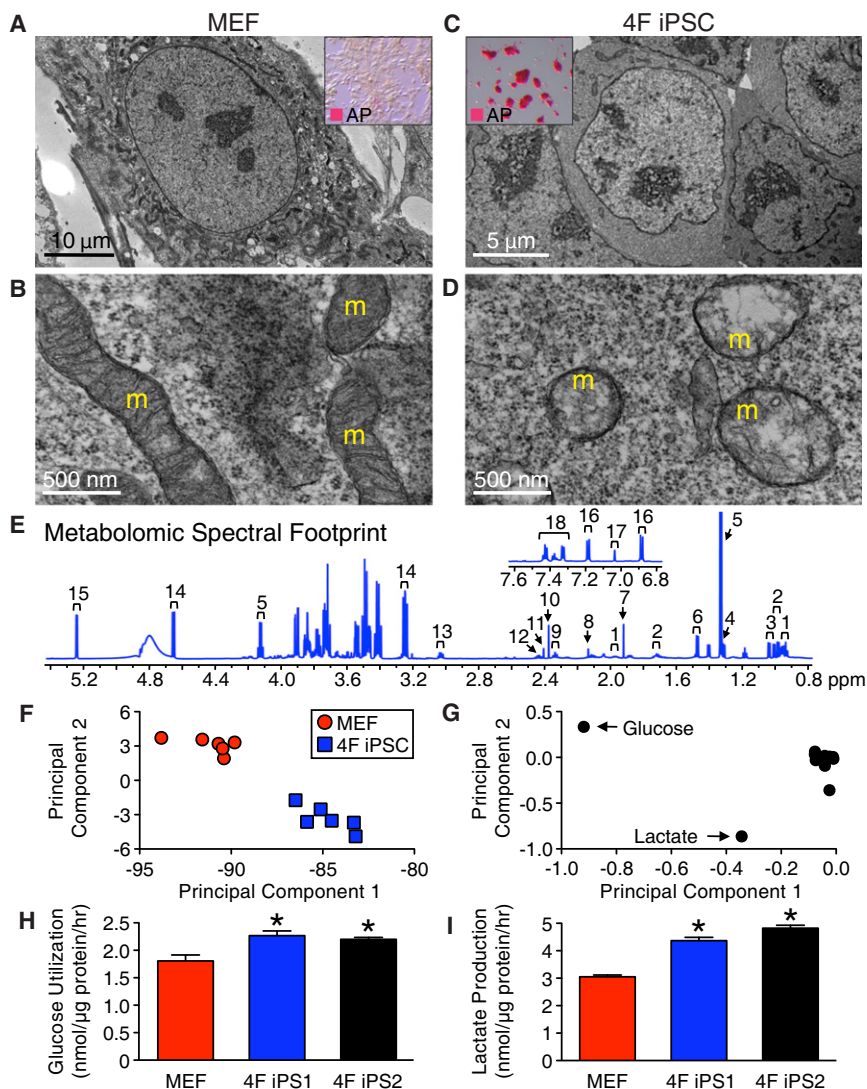
Somatic cells largely depend on mitochondrial oxidative phosphorylation as the primary source of energy production (DeBerardinis et al., 2008). In contrast, embryonic stem cells (ESC) rely on glycolytic ATP generation regardless of oxygen availability (Chung et al., 2007; Kondoh et al., 2007). The reliance on glycolysis reflects a low copy number of mitochondrial DNA (mtDNA) as well as low numbers of nascent mitochondria (St. John et al., 2005; Cho et al., 2006). Differentiation increases mtDNA abundance and promotes mitochondrial biogenesis to form networks of elongated and cristae-rich mitochondria in support of competent oxidative metabolism (Facucho-Oliveira et al., 2007; Chung et al., 2008). Divergent energetic requirements of somatic versus pluripotent phenotypes implicate a distinguishing metabolic profile characterizing dedifferentiation.

We here demonstrate by high-resolution metabolomics that in nuclear reprogramming energy metabolism of iPSC progeny is transformed away from the parental source. Upregulated glycolytic enzymes and downregulated electron transport chain subunits enabled a metabolic switch converting somatic oxidative metabolism into a glycolytic flux-dependent, mitochondria-independent state underlying pluripotent induction.

RESULTS

Transformed Mitochondrial Infrastructure and Metabolomic Profile Define Nuclear Reprogramming

Reprogramming by four stemness transcription factors (4F) restructured mouse embryonic fibroblasts (MEF), characterized by organized mitochondrial networks, to a primordial cytotypic featuring an increased nuclear-to-cytosol ratio with few perinuclear mitochondria (Figures 1A–1D). Mature tubular and cristae-rich somatic mitochondria transitioned into immature spherical and cristae-poor structures in 4F iPSC, indicative of bioenergetic remodeling (Figures 1B and 1D). High-resolution ¹H nuclear magnetic resonance spectroscopy (NMR) quantification of 18 extracellular metabolites (Figure 1E and Figure S1) decoded the metabolic consequences of dedifferentiation by separating the 4F iPSC metabolomic footprint from the parental



MEF landscape (Figure 1F). Accordingly, glucose and lactate were identified as distinguishing metabolites (Figure 1G). Rates of glucose utilization (2.3 ± 0.1 and 2.2 ± 0.1 nmol/μg protein/hr) and lactate production (4.4 ± 0.1 and 4.8 ± 0.1 nmol/μg protein/hr) were significantly elevated in two 4F iPSC lines (4F iPSC1 and 4F iPSC2) compared to MEF (1.8 ± 0.1 and 3.1 ± 0.1 nmol/μg protein/hr, respectively, $n = 6$, $p < 0.05$; Figures 1H and 1I). Thus, nuclear reprogramming induces mitochondrial regression and extracellular metabolome resetting.

Transition from Somatic Oxidative Metabolism to Pluripotent Glycolysis Supports iPSC Derivation

Intracellular metabolite fingerprinting validated the glycolytic capacity of 4F iPSC, segregating the acquired metabolomic pattern away from parental MEF and toward the pluripotent ESC standard (Figure 2A and Figure S1B). The resolved 18 intracellular metabolite panel distinguished iPSC based upon acetate, lactate, fumarate, and taurine concentrations (Figure 2B and Figure S1C). 4F iPSC accumulation of acetate was similar to

Figure 1. Nuclear Reprogramming Transforms Mitochondrial Structure Inducing a Distinct Metabolomic Footprint

Nuclear reprogramming induced regression from elongated and cristae-rich mitochondria (m) of MEFs (A and B) to spherical and cristae-poor remnant structures in four stemness factor-derived iPSCs (4F iPSC) (C and D). Insets demonstrate conversion of fibroblast monolayers (A) into compact clusters (C), which stained for the pluripotency marker alkaline phosphatase (AP). ^1H NMR spectra of extracellular metabolites from 4F iPSC: 1, isoleucine; 2, leucine; 3, valine; 4, threonine; 5, lactate; 6, alanine; 7, acetate; 8, methionine; 9, glutamate; 10, pyruvate; 11, succinate; 12, glutamine; 13, lysine; 14, β -glucose; 15, α -glucose; 16, tyrosine; 17, histidine; and 18, phenylalanine (E). Principal component analysis segregated 4F iPSC metabolomic phenotypes away from the MEF profile with principal component 1 accounting for 88% and 2 for 8% of the total variance (F). The loading plot assigned glucose and lactate as key metabolites contributing to segregation (G). Increased utilization of glucose and production of glycolytic end products in excess of MEF (H and I) were reproduced in independent iPSC lines (4F iPSC1 and 4F iPSC2). Values are mean \pm SEM, $n = 6$. * $p < 0.05$ versus MEF. See also Figure S1.

ESC (31.6 ± 0.9 , 32.5 ± 1.0 , and 29.2 ± 0.7 pmol/μg protein, $n = 3$) and distinct from MEF (21.3 ± 0.5 pmol/μg protein, $n = 3$ populations, $p < 0.05$, Figure 2C). Comparably, lactate was equivalent in 4F iPSC and ESC (127 ± 3 , 152 ± 5 , and 140 ± 10 pmol/μg protein, $n = 3$), yet significantly different from MEF (95 ± 5 pmol/μg protein, $n = 3$, $p < 0.05$; Figure 2D). Lactate efflux (5.3 ± 0.3 and 5.8 ± 0.1 nmol/μg protein/hr) at a rate double that of MEF (2.8 ± 0.2 nmol/μg protein/hr, $n = 6$, $p < 0.05$; Figure 2E) indicated functional glycolysis in 4F iPSC. Consistent with the lower efficiency of glycolytic ATP production compared to oxidative phosphorylation, the ADP/ATP ratio, an index of cellular energy turnover, was reduced in 4F iPSC and ESC compared to MEF (0.046 ± 0.002 , 0.052 ± 0.001 , and 0.053 ± 0.001 versus 0.070 ± 0.001 , respectively, $n = 3$, $p < 0.05$, Figure 2F). Overall, oxygen consumption was low in 4F iPSC and ESC, compared to MEF both at baseline (0.51 ± 0.04 , 0.42 ± 0.07 , and 0.36 ± 0.02 versus 1.8 ± 0.13 nmol/10⁶ cells/min, $n = 3$, $p < 0.05$, Figure 2G) and under electron transport chain uncoupling (0.98 ± 0.10 , 1.22 ± 0.09 , and 0.95 ± 0.13 versus 6.51 ± 1.05 nmol/10⁶ cells/min, $n = 3$, $p < 0.05$, Figure 2H). 4F iPSC preserved the ability to generate mitochondrial membrane potential and demonstrated mitochondrial hyperpolarization (Figures S3A–S3C), indicative of reduced ATP utilization.

Treatment of MEF undergoing reprogramming with 2-deoxyglucose (2DG), a general inhibitor of glycolysis, blunted induction of the pluripotent marker alkaline phosphatase (AP) (Figure 2I),

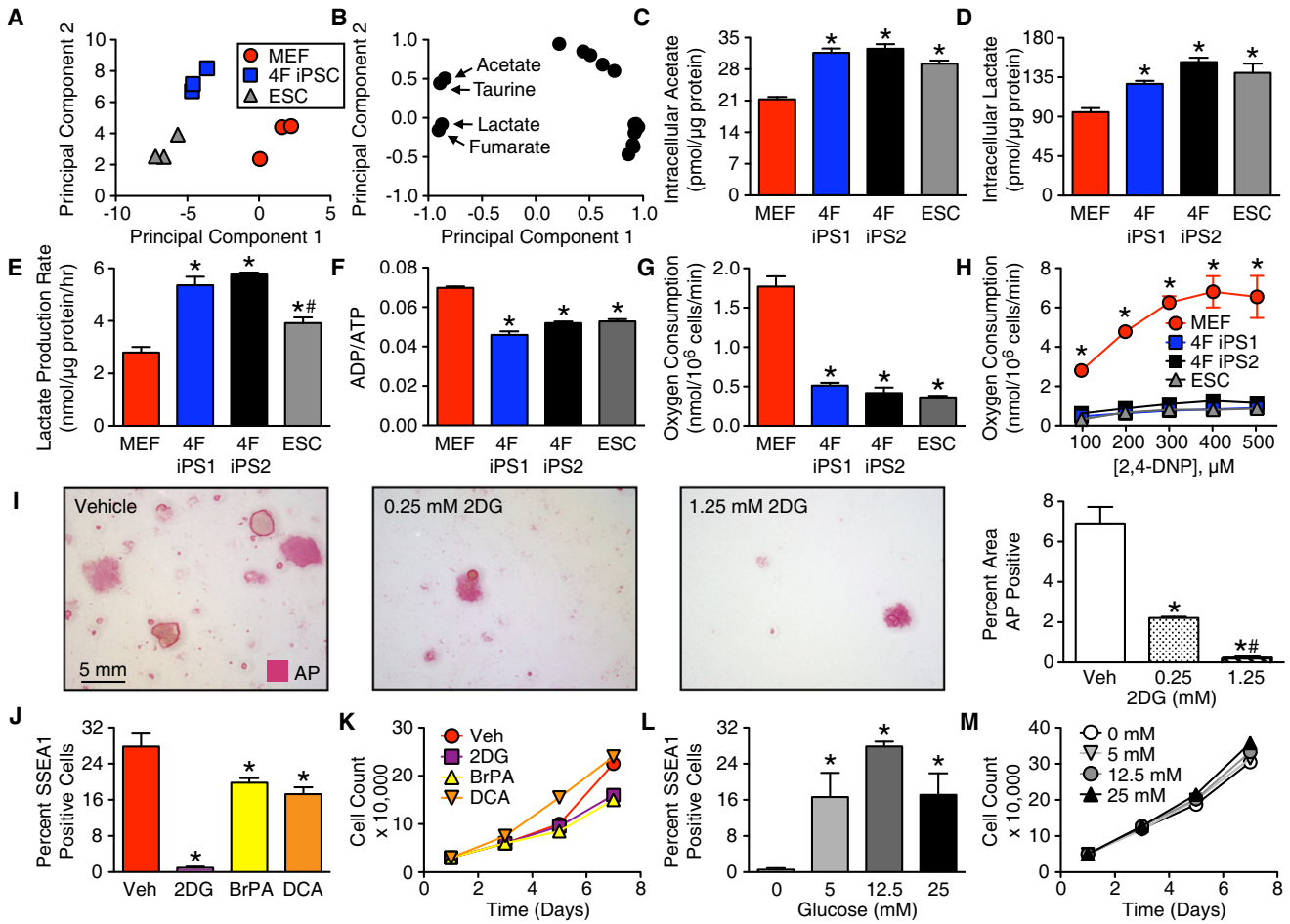


Figure 2. Induction of Pluripotency Requires Functional Glycolysis

¹H NMR fingerprinting of intracellular metabolites segregated 4F iPSC away from MEF and toward ESC (A). The first principal component accounts for 67% and the second for 25% of the total variance. Acetate, taurine, lactate, and fumarate were identified as differentiating metabolites (B). Intracellular concentrations of glycolytic end products were distinct in 4F iPSC compared to MEF and were similar to ESC patterns (C and D). Nuclear reprogramming elevated lactate efflux rates (E) and reduced energy turnover in 4F iPSC, similar to that of ESC (F). Compared to MEF, iPSC and ESC had reduced basal oxygen consumption (G) and lower maximal uncoupled oxidative capacity (H). During reprogramming, the glycolytic inhibitor, 2-deoxyglucose (2DG), blunted induction of the pluripotency marker alkaline phosphatase (I). Glycolytic inhibitors, 1.25 mM 2DG and 100 μM 3-bromopyruvic acid (BrPA) and alternatively a stimulator of oxidative pyruvate disposal, 5 mM dichloroacetate (DCA), reduced reprogramming efficiency, assessed by SSEA1 FACS analysis (J), without altering the growth pattern of MEF (K). Stimulation of glycolysis by elevating extracellular glucose promoted the number of cells achieving the reprogrammed state (L) without altering growth of the parental population (M). Values are mean ± SEM, n = 3 except for lactate efflux, where n = 6. In (A)–(G), *p < 0.05 versus MEF and #p < 0.05 versus 4F iPSC. In (H), *p < 0.05 versus 4F iPSC and ESC. In (I)–(M), *p < 0.05 versus vehicle (Veh) and #p < 0.05 versus 1.25 mM glucose. See also Figure S2.

implicating a glycolytic requirement for iPSC generation. Beyond 2DG, the hexokinase 2 inhibitor 3-bromopyruvic acid (BrPA) (Ko et al., 2001) and pyruvate dehydrogenase kinase inhibitor dichloroacetate (DCA) (Stacpool, 1989) reduced reprogramming efficiency (0.9% ± 0.3% in 2DG, 19.8% ± 1.0% in BrPA, 17.3% ± 1.5% in DCA versus 27.8% ± 3.1% SSEA1-positive cells in vehicle, n = 3, p < 0.05, Figure 2J) without impairing cell growth (Figure 2K). Extracellular metabolite profiles of MEF treated with 2DG or BrPA were consistent with inhibition of glycolysis and stimulation of oxidative metabolism, while DCA treatment stimulated mitochondrial function and accelerated consumption of oxidative substrates (Figures S2A–S2C). Glucose supplementation stimulated glycolytic flux, reduced mitochondrial function (Figures S2D–S2F), and increased

SSEA1-positive cell density (0.5% ± 0.3%, 16.6% ± 5.3%, 27.8% ± 1.1%, and 17.1% ± 4.7% SSEA1-positive cells in 0, 5, 12.5, and 25 mM glucose, n = 3, p < 0.05). Conversely, few MEFs underwent nuclear reprogramming in the absence of glucose (Figures 2L and 2M). Transition from somatic oxidative metabolism to pluripotent glycolysis thus contributes to nuclear reprogramming efficiency.

Glycolytic Flux Fuels Pluripotent Induction

Mitochondrial membrane potential served as a surrogate of metabolic transition during nuclear reprogramming. Prospective live cell imaging distinguished ESC-like compact clusters with high tetramethylrhodamine methyl ester (TMRM) fluorescence from transfected nonreprogrammed MEF with low

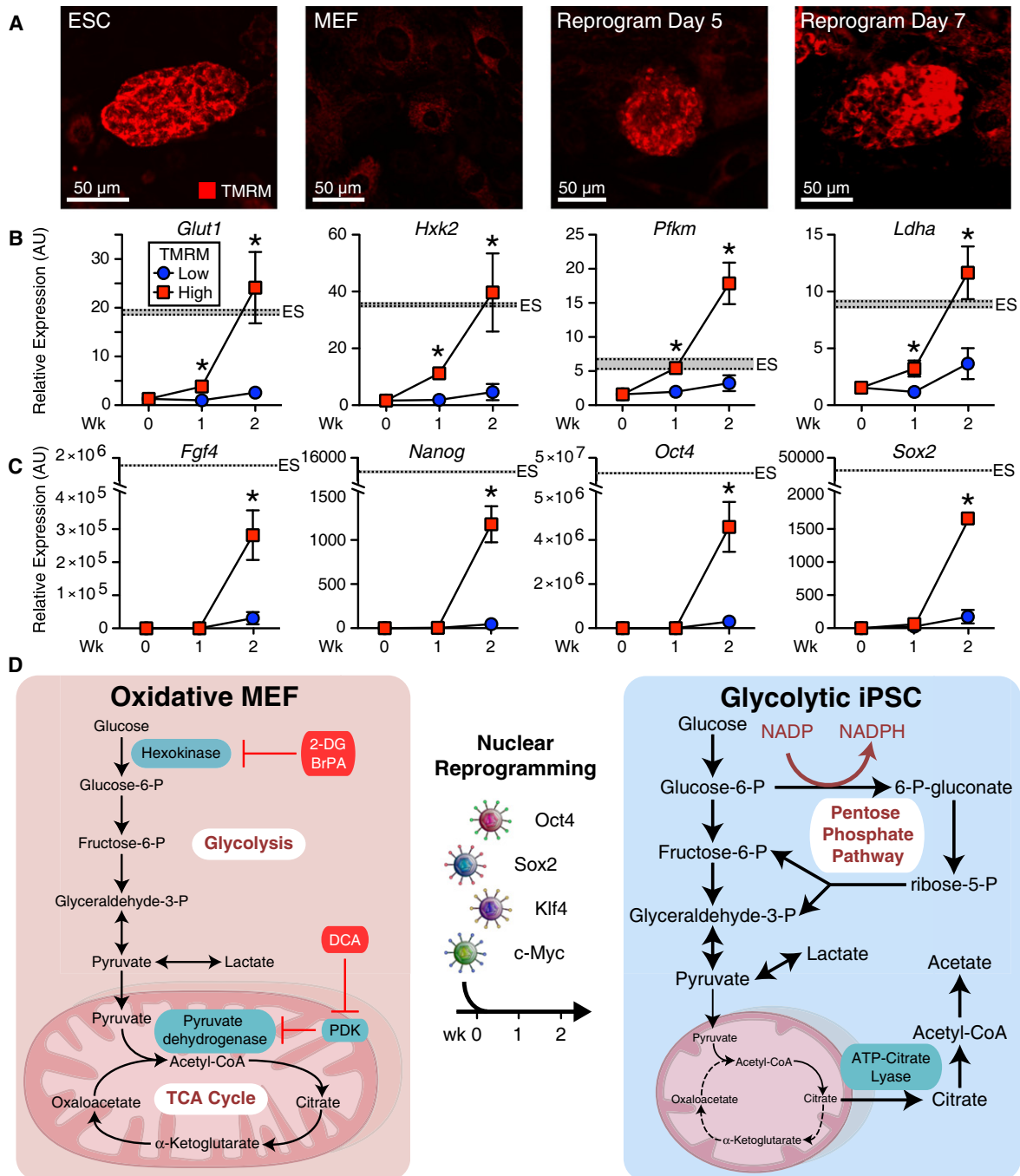


Figure 3. Glycolytic Engagement Mobilizes Pluripotent Gene Induction

Similar to ESC and distinct from MEF, live cell imaging of mitochondrial membrane potential identified nascent compact cell clusters with high TMRM fluorescence within 5–7 days of nuclear reprogramming (A). Compared to the low TMRM fluorescence population, high-fluorescence cells had significantly elevated glycolytic gene expression (*Glut1*, *Hxk2*, *Pfkf*, and *Ldha*) within 1 week of reprogramming, which by 2 weeks of reprogramming equaled ESC glycolytic gene expression (B). Of note, at week 1 of reprogramming, pluripotent gene expression (*Fgf4*, *Nanog*, *Oct4*, and *Sox2*) remained low in high TMRM fluorescence cells, similar to the starting MEF, with pluripotent gene induction apparent during the second week (C). Shaded region represents mean \pm SEM for ESC gene expression. Values are mean \pm SEM, n = 3. *p < 0.05 versus low TMRM population. Nuclear reprogramming switches oxidative MEF into glycolytic iPSC (D). See also Figure S3.

mitochondrial membrane fluorescence (Figure 3A). FACS sampling of high TMRM cells at days 7 and 14 selected an emergent subpopulation within small cell clusters, consistent with

mitochondrial membrane potential polarization during dedifferentiation (Figures S3A–S3D). At day 7, high TMRM cells had significantly elevated glycolytic gene expression (*Glut1*, *Hxk2*,

Pfkm, and *Ldha*), which met that of ESC by 2 weeks of reprogramming (Figure 3B). In contrast, at 1 week of reprogramming, pluripotent gene expression (*Fgf4*, *Nanog*, *Oct4*, and *Sox2*) remained low in high TMRM cells, similar to starting MEF, with pluripotent gene induction apparent only after 2 weeks (Figure 3C). Metabolic reprogramming thus precedes pluripotent gene expression during somatic cell dedifferentiation from an oxidative to a glycolytic iPSC phenotype (Figure 3D).

Reprogramming-Induced Metabolic Remodeling Independent of *c-Myc* Induction

As *c-Myc* gene targets control rates of glycolysis and mitochondrial biogenesis (Dang, 2007), a cell line was derived without *c-Myc* (3F iPSC). Similar to 4F iPSC, NMR metabolomic fingerprinting and fingerprinting segregated 3F iPSC away from parental MEF (Figures 4A and 4B), based upon greater intracellular and extracellular accumulation of glycolytic end products, acetate (intracellular, 30.4 ± 0.8 versus 21.3 ± 0.5 pmol/ μ g protein; extracellular, 0.41 ± 0.03 versus 0.035 ± 0.001 nmol/ μ g protein/hr, $n = 3$, $p < 0.05$, Figure 4C) and lactate (intracellular, 188 ± 11 versus 95 ± 5 pmol/ μ g protein; extracellular, 4.1 ± 0.1 versus 3.0 ± 0.1 nmol/ μ g protein/hr, $n = 3$, $p < 0.05$, Figure 4D). Consistent with accelerated glycolysis, 3F iPSC displayed reduced energy turnover compared to MEF (0.039 ± 0.005 versus 0.068 ± 0.006 , $n = 3$, $p < 0.05$, Figure 4E). Both 3F and 4F iPSC demonstrated limited oxidative capacity and elevated lactate production (Figure 4F). Thus, nuclear reprogramming-induced metabolic remodeling is characteristic of the iPSC phenotype, independent of *c-Myc* transduction.

iPS Metabotype Arises through Proteome Restructuring

Metaboproteome dissection delineated a transformed molecular signature in iPSC, distinct from parental MEF yet synonymous to the metabolic protein profile of ESC (Figures 4G–4J, Figure S4, Table S1 and Table S2). A label-free, quantitative proteomics approach revealed the identities of glycolytic enzymes consistently upregulated in pluripotent cytotypes relative to MEF (Figure 4G and Figure S4A), confirmed independently by 2D gel-based analysis (Figure 4I). Concomitantly, 65% of detected complex 1 subunits were downregulated in iPSC extracts (Figure 4H and Figure S4B, Table S1) as validated by 2D gel-based analysis (Figure 4J), underscoring departure from MEF patterns and acquisition of a glycolytic-dependent profile (Figure 4K). In addition, reprogramming was associated with selective downregulation of the reducing equivalent entry points (complex I and II) (Figure S4C, Table S1). Thus, the resolved iPSC metaboproteome unmask a bioenergetic switch in energy production infrastructure underlying metabolic remodeling in nuclear reprogramming.

DISCUSSION

Nuclear reprogramming sets in motion dedifferentiation processes leading to acquisition of pluripotency. This study resolved the metabolic attributes underpinning iPSC generation. Metaboproteome restructuring was demonstrated to underlie conversion from somatic oxidative bioenergetics to glycolysis of pluripotent progeny. Promotion of a glycolytic flux-dependent, mitochondria-independent metabotype fostered nuclear reprogramming.

Regression of the parental somatic network of abundant tubular and cristae-rich mitochondria into sparse spherical and cristae-poor structures characterized iPSC progeny. A mitochondria-poor capacity would enable iPSC to revert reactive oxygen species-dependent telomere shortening associated with cellular aging (Passos et al., 2007; Marion et al., 2009). In fact, mitochondrial regression and reduction of mtDNA as a result of nuclear reprogramming are consistent with the undeveloped mitochondrial morphology of ESC (Kondoh et al., 2007; Armstrong et al., 2010; Prigione et al., 2010; Zeuschner et al., 2010). Induced reduction in mitochondria number and maturity suggests metamorphosis of the bioenergetic infrastructure underlying dedifferentiation.

Metabolomic fingerprinting and fingerprinting indeed demonstrated distinct features of iPSC metabolism. The key metabolic rates contributing to the iPSC phenotype were consistent among multiple clones, and included elevated utilization of glucose and accumulation of intracellular and extracellular lactate (via lactate dehydrogenase) and acetate (via acetyl-CoA synthase or ATP-citrate lyase), suggesting that accelerated glycolysis results in accumulation of metabolic byproducts within the cell, followed by metabolite exportation. iPSC demonstrated diminished basal oxygen consumption and uncoupled oxidative capacity, indicating departure from oxidative metabolism. ESCs also rely on glycolytic ATP generation (Cho et al., 2006; Facucho-Oliveira et al., 2007), with pluripotency maintenance sustained under hypoxic conditions (Ezashi et al., 2005). Acquisition of an embryonic-like metabolic state is concomitant with global transcriptional and epigenetic reorganization that includes demethylation and activation of the promoter region of pluripotency inducers (Bock et al., 2011; Plath and Lowry, 2011). A glycolytic burst could promote linkage of energy metabolism with nuclear reprogramming-induced epigenetic resetting (Huangfu et al., 2008; Friis et al., 2009; Wellen et al., 2009; Teperino et al., 2010), priming the cell for pluripotent induction. Indeed, expression of glycolytic genes preceded pluripotent gene expression, implicating metabolic remodeling as a facilitator of nuclear reprogramming.

Complete oxidation of glucose limits generation of substrates for biosynthetic pathways. Transition to glycolytic metabolism would fuel specific cellular processes, such as ATP consumption in the cell nucleus, and provide the necessary balance between ATP generation and production of metabolic precursors to meet anabolic requirements of dedifferentiation and associated proliferation (DeBerardinis et al., 2008; Chung et al., 2010). Strategies that in part stimulate glycolysis, including induction of hypoxia or inhibition of the p53 pathway, increase nuclear reprogramming efficiency (Kruse and Gu, 2006; Krizhanovsky and Lowe, 2009; Yoshida et al., 2009). Consistent with the ability of small molecules with known metabolic targets to modulate the appearance of pluripotent colonies (Zhu et al., 2010), here stimulation of glycolytic flux potentiated reprogramming, whereas oxidative metabolism promotion preserved the somatic cytotype.

c-Myc, through its regulation of both glycolysis and mitochondrial metabolism, is a key contributor to the metabolic Warburg effect, reflecting the tendency of highly proliferative cell types to convert glucose to lactate despite sufficient oxygen for mitochondrial oxidative metabolism (Dang, 2007). Here 3F iPSC displayed equivalent metabolic profiles to 4F iPSC counterparts,

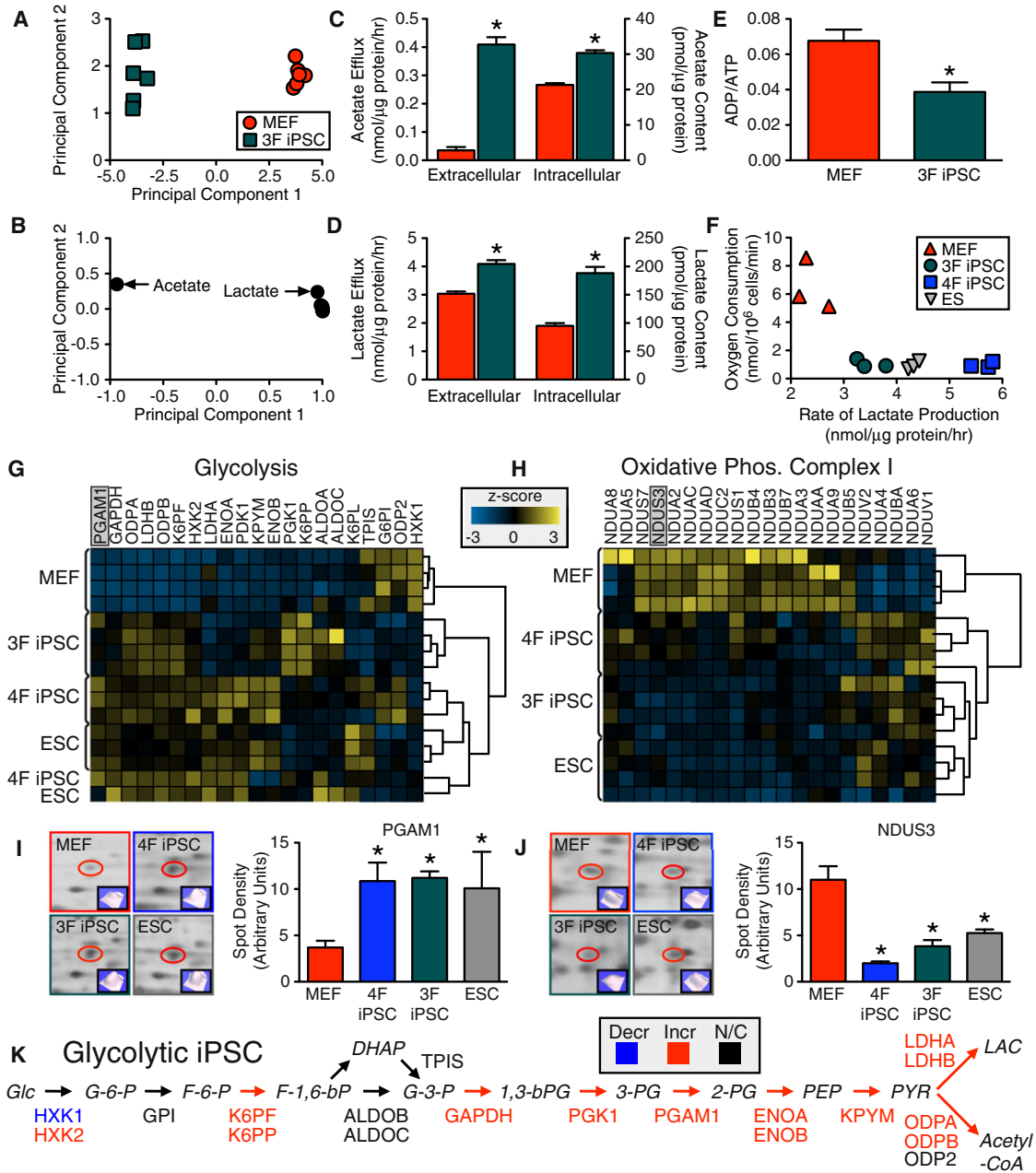


Figure 4. Metabolic Reprogramming Is Independent of *c-Myc* Transduction and Supported by Glycolytic/Electron Transport Chain Proteome Switch

¹H NMR cellular metabolomic fingerprints (n = 6) of three stemness factor-induced iPSC (3F iPSC) segregated, away from the somatic, the acquired pattern (first principal component accounts for 97% and second for 1% of total variance) (A). Glycolytic end products, acetate and lactate, were key metabolites responsible for segregation (B). Intracellular content and efflux of acetate and lactate were significantly elevated in the 3F iPSC compared to MEF (C and D) and associated with reduced energy turnover (n = 6) (E). Compared to MEF, 3F iPSC had lower maximal oxidative capacity and higher lactate production similar to that of ESC, albeit not fully overlapping with 4F iPSC (n = 3) (F). Proteome-wide label-free quantification segregated iPSC away from MEF toward an ESC pattern based on agglomerative clustering of z score transformed data (n = 4) due to predominant glycolytic enzyme upregulation (G). Electron transport chain complex I subunits were predominantly downregulated in pluripotent cytotypes, which clustered away from MEF (H). 2D gel quantification and MS/MS identification (n = 3) independently confirmed glycolytic upregulation (I) and complex I downregulation (J). iPSC proteomic upregulation was mapped across the glycolytic pathway (K). Values are mean ± SEM. *p < 0.05 versus MEF. Proteins are abbreviated by Swiss-Prot gene name. See also Figure S4 and Table S1 and Table S2.

verifying that nuclear reprogramming-induced metabolic remodeling did not require *c-Myc* transduction. Proteomic dissection resolved a metabolic infrastructure that distinguished 3F and

4F iPSC from fibroblasts. Specifically, reprogramming induced reciprocal changes in glycolytic enzymes and electron transport chain components, indicating a molecular substrate contributing

to the switch from oxidative to glycolytic metabolism. The observed decreased expression of complex I and II subunits would uncouple oxidative metabolism and ATP generation, favoring glycolytic-dependent ATP production.

In summary, dedifferentiation of parental somatic cells induced mitochondrial regression, electron transport chain down-regulation, and glycolysis enzyme upregulation, revealing a pluripotent glycolytic signature with limited dependence on mitochondrial metabolism. Induction of the glycolytic metabolite supports anabolic and catabolic requirements for bona fide pluripotency to regulate cell fate.

EXPERIMENTAL PROCEDURES

Transduction

Mouse embryonic fibroblasts were transduced with in-house HIV-based viral vectors encoding OCT3/4, SOX2, and KLF4 in the presence or absence of c-MYC to produce iPSC clones that met pluripotent criteria including expression of stem cell markers, embryoid body differentiation, teratoma formation, diploid aggregation, and contribution to organogenesis (Martinez-Fernandez et al., 2009; Nelson et al., 2009a, 2009b). Alternatively, iPSCs were derived with a viPS (Open Biosystems) kit. iPSCs and mouse ESCs (R1) were induced and maintained in DMEM supplemented with 15% FBS, 25 mM glucose, 2 mM Glutamax (Invitrogen), and 1 mM sodium pyruvate. Reprogramming efficiency was quantified using an alkaline phosphatase staining kit (Stemgent) or FACS analysis of SSEA1 expression (Millipore) on a LSR II flow cytometer.

Ultrastructure

Mitochondrial density and morphology were evaluated in 1% glutaraldehyde and 4% formaldehyde fixed cells and examined as ultramicrotome sections on a JEOL 1200 EXII electron microscope (Perez-Terzic et al., 2007).

Metabolomic Footprinting and Fingerprinting

For footprinting of extracellular metabolites (see the Supplemental Experimental Procedures), 540 μ l of media collected following 24 hr of culture was added to 60 μ l of D₂O (Sigma) containing 5 mM sodium 3-(trimethylsilyl)propionate-2,2,3,3-d₄ (TSP) (Sigma) for chemical shift reference and 81.84 mM formate (Sigma) for peak quantification reference (Turner et al., 2008). For intracellular metabolite fingerprinting, neutralized perchloric acid extracts were concentrated with a SpeedVac and suspended in 600 μ l of 100 mM phosphate buffer (pH 7.0) in D₂O (Sigma) containing 0.5 mM TSP (Beckonert et al., 2007). Identities of ¹H NMR spectra peaks obtained on a Bruker Ultra-shield 700 MHz spectrometer with a *zgpr* water suppression presaturation pulse were assigned by comparison to reference values for chemical shift and multiplicity, and confirmed by comparison to spectra of pure compounds in the Human Metabolome Database (Govindaraju et al., 2000; Wishart et al., 2009).

Metabolites and Oxygen Consumption

Lactate efflux rate was assessed in extracellular media using a lactate assay (SUNY). Nucleotide concentrations were determined in neutralized perchloric acid extracts by high-performance liquid chromatography, using a 0.1 M phosphate (pH 6.5), 0.01 M tetrabutylammoniumhydrogensulfate, and 40% methanol elution buffer (Chung et al., 2007). Oxygen consumption was assessed using an electrode system (Hansatech) on 5 million trypsinized cells suspended in DMEM. Maximal rate of uncoupled oxygen consumption was assessed by serial additions of 2,4-dinitrophenol (Sigma).

TMRM Fluorescence Sorting and Gene Expression

Mitochondrial membrane potential was assessed at day 4–14 of reprogramming by incubating with 20 nM TMRM (Anaspec) for 30 min at 37°C, and imaged with a LSM 510 Axiovert laser confocal microscope. By 1 and 2 weeks of reprogramming, single-cell suspensions were incubated in TMRM and separated by a FACS Aria Cell Sorter. Gene expression was examined on an Eco RT-PCR system (Illumina).

Proteomics

Protein extracts were resolved by 2D gel electrophoresis and 4%–15% SDS-PAGE (100 and 30 μ g, respectively) and silver stained (Zlatkovic-Lindor et al., 2010). For comparative analysis, SDS-PAGE lanes were excised, destained, and prepared for LC-MS/MS, as were protein species from 2D gels identified as significantly altered by PDQuest analysis (Zlatkovic-Lindor et al., 2010). Isolated tryptic peptides were analyzed and identified by LTQ-Orbitrap mass spectrometry. Label-free quantitative comparison of SDS-PAGE protein and peptide abundance was carried out on acquired MS spectra using Rosetta Elucidator's differential workflow, with annotation performed using Peptide-Teller and ProteinTeller (Neubert et al., 2008; Lomenick et al., 2009). See the Supplemental Experimental Procedures.

Statistical Analysis

Data are presented as mean \pm SEM. Metabolic footprinting and fingerprinting were analyzed by principal component analysis using JMP. Student's t test was used to evaluate two group comparisons and ANOVA with a Bonferroni post-hoc correction for three group comparisons. A value of $p < 0.05$ was considered significant.

SUPPLEMENTAL INFORMATION

Supplemental Information includes four figures, two tables, Supplemental Experimental Procedures, and Supplemental References and can be found with this article online at doi:10.1016/j.cmet.2011.06.011.

ACKNOWLEDGMENTS

The authors thank Mayo Clinic Nuclear Magnetic Resonance Core and Flow Cytometry/Optical Morphology Shared Resource for assistance. This work was supported by the National Institutes of Health (R01HL083439, T32HL007111, R01HL085208, R56AI074363), Canadian Institutes of Health Research, Marriott Program, and Mayo Clinic.

Received: October 18, 2010

Revised: May 1, 2011

Accepted: June 9, 2011

Published: August 2, 2011

REFERENCES

- Armstrong, L., Tilgner, K., Saretzki, G., Atkinson, S.P., Stojkovic, M., Moreno, R., Przyborski, S., and Lako, M. (2010). Human induced pluripotent stem cell lines show similar stress defence mechanisms and mitochondrial regulation to human embryonic stem cells. *Stem Cells* 28, 661–673.
- Beckonert, O., Keun, H.C., Ebbels, T.M., Bundy, J., Holmes, E., Lindon, J.C., and Nicholson, J.K. (2007). Metabolic profiling, metabolomic and metabolomic procedures for NMR spectroscopy of urine, plasma, serum and tissue extracts. *Nat. Protoc.* 2, 2692–2703.
- Bock, C., Kiskinis, E., Verstappen, G., Gu, H., Boulting, G., Smith, Z.D., Ziller, M., Croft, G.F., Amoroso, M.W., Oakley, D.H., et al. (2011). Reference maps of human ES and iPS cell variation enable high-throughput characterization of pluripotent cell lines. *Cell* 144, 439–452.
- Cho, Y.M., Kwon, S., Pak, Y.K., Seol, H.W., Choi, Y.M., Park do, J., Park, K.S., and Lee, H.K. (2006). Dynamic changes in mitochondrial biogenesis and antioxidant enzymes during the spontaneous differentiation of human embryonic stem cells. *Biochem. Biophys. Res. Commun.* 348, 1472–1478.
- Chung, S., Dzeja, P.P., Faustino, R.S., Perez-Terzic, C., Behfar, A., and Terzic, A. (2007). Mitochondrial oxidative metabolism is required for the cardiac differentiation of stem cells. *Nat. Clin. Pract. Cardiovasc. Med.* 4 (Suppl 1), S60–S67.
- Chung, S., Dzeja, P.P., Faustino, R.S., and Terzic, A. (2008). Developmental restructuring of the creatine kinase system integrates mitochondrial energetics with stem cell cardiogenesis. *Ann. N Y Acad. Sci.* 1147, 254–263.

- Chung, S., Arrell, D.K., Faustino, R.S., Terzic, A., and Dzeja, P.P. (2010). Glycolytic network restructuring integral to the energetics of embryonic stem cell cardiac differentiation. *J. Mol. Cell. Cardiol.* **48**, 725–734.
- Dang, C.V. (2007). The interplay between MYC and HIF in the Warburg effect. *Ernst Schering Found. Symp. Proc.*, 35–53.
- DeBerardinis, R.J., Lum, J.J., Hatzivassiliou, G., and Thompson, C.B. (2008). The biology of cancer: metabolic reprogramming fuels cell growth and proliferation. *Cell Metab.* **7**, 11–20.
- Dzeja, P.P., Chung, S., Faustino, R.S., Behfar, A., and Terzic, A. (2011). Developmental enhancement of adenylate kinase-AMPK metabolic signaling axis supports stem cell cardiac differentiation. *PLoS ONE* **6**, e19300. 10.1371/journal.pone.0019300.
- Ezashi, T., Das, P., and Roberts, R.M. (2005). Low O₂ tensions and the prevention of differentiation of hES cells. *Proc. Natl. Acad. Sci. USA* **102**, 4783–4788.
- Facucho-Oliveira, J.M., Alderson, J., Spikings, E.C., Egginton, S., and St John, J.C. (2007). Mitochondrial DNA replication during differentiation of murine embryonic stem cells. *J. Cell Sci.* **120**, 4025–4034.
- Friis, R.M., Wu, B.P., Reinke, S.N., Hockman, D.J., Sykes, B.D., and Schultz, M.C. (2009). A glycolytic burst drives glucose induction of global histone acetylation by picNuA4 and SAGA. *Nucleic Acids Res.* **37**, 3969–3980.
- Govindaraju, V., Young, K., and Maudsley, A.A. (2000). Proton NMR chemical shifts and coupling constants for brain metabolites. *NMR Biomed.* **13**, 129–153.
- Huangfu, D., Maehr, R., Guo, W., Eijkelenboom, A., Snitow, M., Chen, A.E., and Melton, D.A. (2008). Induction of pluripotent stem cells by defined factors is greatly improved by small-molecule compounds. *Nat. Biotechnol.* **26**, 795–797.
- Ko, Y.H., Pedersen, P.L., and Geschwind, J.F. (2001). Glucose catabolism in the rabbit VX2 tumor model for liver cancer: characterization and targeting hexokinase. *Cancer Lett.* **173**, 83–91.
- Kondoh, H., Leonart, M.E., Nakashima, Y., Yokode, M., Tanaka, M., Bernard, D., Gil, J., and Beach, D. (2007). A high glycolytic flux supports the proliferative potential of murine embryonic stem cells. *Antioxid. Redox Signal.* **9**, 293–299.
- Krizhanovsky, V., and Lowe, S.W. (2009). Stem cells: the promises and perils of p53. *Nature* **460**, 1085–1086.
- Kruse, J.P., and Gu, W. (2006). p53 aerobics: the major tumor suppressor fuels your workout. *Cell Metab.* **4**, 1–3.
- Lomenick, B., Hao, R., Jonai, N., Chin, R.M., Aghajani, M., Warburton, S., Wang, J., Wu, R.P., Gomez, F., Loo, J.A., et al. (2009). Target identification using drug affinity responsive target stability (DARTS). *Proc. Natl. Acad. Sci. USA* **106**, 21984–21989.
- Marion, R.M., Strati, K., Li, H., Tejera, A., Schoeftner, S., Ortega, S., Serrano, M., and Blasco, M.A. (2009). Telomeres acquire embryonic stem cell characteristics in induced pluripotent stem cells. *Cell Stem Cell* **4**, 141–154.
- Martinez-Fernandez, A., Nelson, T.J., Yamada, S., Reyes, S., Alekseev, A.E., Perez-Terzic, C., Ikeda, Y., and Terzic, A. (2009). iPS programmed without c-MYC yield proficient cardiogenesis for functional heart chimerism. *Circ. Res.* **105**, 648–656.
- Meissner, A., Wernig, M., and Jaenisch, R. (2007). Direct reprogramming of genetically unmodified fibroblasts into pluripotent stem cells. *Nat. Biotechnol.* **25**, 1177–1181.
- Nelson, T.J., Martinez-Fernandez, A., Yamada, S., Mael, A.A., Terzic, A., and Ikeda, Y. (2009a). Induced pluripotent reprogramming from promiscuous human stemness-related factors. *Clin. Transl. Sci.* **2**, 118–126.
- Nelson, T.J., Martinez-Fernandez, A., Yamada, S., Perez-Terzic, C., Ikeda, Y., and Terzic, A. (2009b). Repair of acute myocardial infarction by human stemness factors induced pluripotent stem cells. *Circulation* **120**, 408–416.
- Nelson, T.J., Martinez-Fernandez, A., and Terzic, A. (2010). Induced pluripotent stem cells: developmental biology to regenerative medicine. *Nat. Rev. Cardiol.* **7**, 700–710.
- Neubert, H., Bonnett, T.P., Rumpel, K., Hunt, B.T., Henle, E.S., and James, I.T. (2008). Label-free detection of differential protein expression by LC/MALDI mass spectrometry. *J. Proteome Res.* **7**, 2270–2279.
- Passos, J.F., Saretzki, G., Ahmed, S., Nelson, G., Richter, T., Peters, H., Wappler, I., Birket, M.J., Harold, G., Schaeuble, K., et al. (2007). Mitochondrial dysfunction accounts for the stochastic heterogeneity in telomere-dependent senescence. *PLoS Biol.* **5**, e110. 10.1371/journal.pbio.0050110.
- Perez-Terzic, C., Faustino, R.S., Boorsma, B.J., Arrell, D.K., Niederlander, N.J., Behfar, A., and Terzic, A. (2007). Stem cells transform into a cardiac phenotype with remodeling of the nuclear transport machinery. *Nat. Clin. Pract. Cardiovasc. Med.* **4** (Suppl 1), S68–S76.
- Plath, K., and Lowry, W.E. (2011). Progress in understanding reprogramming to the induced pluripotent state. *Nat. Rev. Genet.* **12**, 253–265.
- Prigione, A., Fauler, B., Lurz, R., Lehrach, H., and Adjaye, J. (2010). The senescence-related mitochondrial/oxidative stress pathway is repressed in human induced pluripotent stem cells. *Stem Cells* **28**, 721–733.
- Stacpoole, P.W. (1989). The pharmacology of dichloroacetate. *Metabolism* **38**, 1124–1144.
- St. John, J.C., Ramalho-Santos, J., Gray, H.L., Petrosko, P., Rawe, V.Y., Navara, C.S., Simerly, C.R., and Schatten, G.P. (2005). The expression of mitochondrial DNA transcription factors during early cardiomyocyte in vitro differentiation from human embryonic stem cells. *Cloning Stem Cells* **7**, 141–153.
- Takahashi, K., and Yamanaka, S. (2006). Induction of pluripotent stem cells from mouse embryonic and adult fibroblast cultures by defined factors. *Cell* **126**, 663–676.
- Teperino, R., Schoonjans, K., and Auwerx, J. (2010). Histone methyl transferases and demethylases; can they link metabolism and transcription? *Cell Metab.* **12**, 321–327.
- Turner, W.S., Seagle, C., Galanko, J.A., Favorov, O., Prestwich, G.D., Macdonald, J.M., and Reid, L.M. (2008). Nuclear magnetic resonance metabolomic footprinting of human hepatic stem cells and hepatoblasts cultured in hyaluronan-matrix hydrogels. *Stem Cells* **26**, 1547–1555.
- Wellen, K.E., Hatzivassiliou, G., Sachdeva, U.M., Bui, T.V., Cross, J.R., and Thompson, C.B. (2009). ATP-citrate lyase links cellular metabolism to histone acetylation. *Science* **324**, 1076–1080.
- Wishart, D.S., Knox, C., Guo, A.C., Eisner, R., Young, N., Gautam, B., Hau, D.D., Psychogios, N., Dong, E., Bouatra, S., et al. (2009). HMDB: a knowledge-base for the human metabolome. *Nucleic Acids Res.* **37**, D603–D610.
- Yoshida, Y., Takahashi, K., Okita, K., Ichisaka, T., and Yamanaka, S. (2009). Hypoxia enhances the generation of induced pluripotent stem cells. *Cell Stem Cell* **5**, 237–241.
- Zeuschner, D., Mildner, K., Zaehres, H., and Scholer, H.R. (2010). Induced pluripotent stem cells at nanoscale. *Stem Cells Dev.* **19**, 615–620.
- Zhu, S., Li, W., Zhou, H., Wei, W., Ambasadhan, R., Lin, T., Kim, J., Zhang, K., and Ding, S. (2010). Reprogramming of human primary somatic cells by OCT4 and chemical compounds. *Cell Stem Cell* **7**, 651–655.
- Zlatkovic-Lindor, J., Arrell, D.K., Yamada, S., Nelson, T.J., and Terzic, A. (2010). ATP-sensitive K⁺ channel-deficient dilated cardiomyopathy proteome remodeled by embryonic stem cell therapy. *Stem Cells* **28**, 1355–1367.